

Bound in continuum states and induced transparency in mesoscopic demultiplexer with two outputs

Z Labdouti, T Mrabti, A Mouadili, E H El Boudouti, F Fethi, and B Djafari-Rouhani

Citation: Chin. Phys. B, 2020, 29 (**12**): 127301. DOI: 10.1088/1674-1056/abad23

Journal homepage: http://cpb.iphy.ac.cn; http://iopscience.iop.org/cpb

What follows is a list of articles you may be interested in

Progress on band structure engineering of twisted bilayer and two-dimensional moir\'e heterostructures

Wei Yao(姚维), Martin Aeschlimann, and Shuyun Zhou(周树云)

Chin. Phys. B, 2020, 29 (**12**): 127304. DOI: 10.1088/1674-1056/abc7b6

Bound in continuum states and induced transparency in mesoscopic demultiplexer with two outputs

Z Labdouti, T Mrabti, A Mouadili, E H El Boudouti, F Fethi, and B Djafari-Rouhani

Chin. Phys. B, 2020, 29 (**12**): 127301. DOI: 10.1088/1674-1056/abad23

Progress on 2D topological insulators and potential applications in electronic devices

Yanhui Hou(侯延辉), Teng Zhang(张腾), Jiatao Sun(孙家涛), Liwei Liu(刘立巍), Yugui Yao(姚裕贵), Yeliang Wang(王业亮)

Chin. Phys. B, 2020, 29 (**9**): 097304. DOI: 10.1088/1674-1056/aba9c5

Time-dependent first-principles study of optical response of $BaTiO_3$ quantum dots coupled with silver nanowires

Bo-Xun Han(韩博逊), Hong Zhang(张红)

Chin. Phys. B, 2019, 28 (**6**): 067301. DOI: 10.1088/1674-1056/28/6/067301

Manipulating coupling state and magnetism of Mn-doped ZnO nanocrystals by changing the coordination environment of Mn via hydrogen annealing

Yan Cheng(程岩), Wen-Xian Li(李文献), Wei-Chang Hao(郝维昌), Huai-Zhe Xu(许怀哲), Zhong-Fei Xu(徐忠菲), Li-Rong Zheng(郑离荣), Jing Zhang(张静),Shi-Xue Dou(窦士学), Tian-Min Wang(王天民)

Chin. Phys. B, 2016, 25 (**1**): 017301. DOI: 10.1088/1674-1056/25/1/017301

Bound in continuum states and induced transparency in mesoscopic demultiplexer with two outputs

Z Labdouti[1], T Mrabti[2,†], A Mouadili[3], E H El Boudouti[1], F Fethi[1], and B Djafari-Rouhani[4]

[1] *LPMR, Département de Physique, Faculté des Sciences, Université Mohammed I, Oujda, Morocco*
[2] *LSTA, Département de Physique, Faculté Polydisciplinaire de Larache, Université Abdelmalek Essaadi, Tétouan, Morocco*
[3] *LPMCER, Département de Physique, Faculté des Sciences et Techniques de Mohammedia, Université Hassan II, Casablanca, Morocco*
[4] *IEMN, UMR CNRS* 8520, *UFR de Physique, Université de Lille,* 59655 *Villeneuve d'Ascq, France*

(Received 31 May 2020; revised manuscript received 21 July 2020; accepted manuscript online 7 August 2020)

We investigate the electronic transport in a simple mesoscopic cross structure made of two wires (stubs) grafted at the same point along a quantum waveguide. We show that the structure may exhibit important phenomena such as bound in continuum (BIC) states. These states are transformed into electromagnetically induced transparency (EIT) resonance by detuning slightly the lengths of the stubs. The last phenomenon is used to propose and study a mesoscopic demultiplexer device with an input waveguide and two output waveguides. We give closed-form expressions of the geometrical parameters that allow a selective transfer of a given state in the first waveguide without perturbing the second waveguide. The effect of temperature on the transmission resonances is also examined by using Landauer–Büttiker formula. The analytical results of the dispersion relation and transmission and reflection coefficient are obtained using the Green's function method.

Keywords: mesoscopic structure, demultiplexer device, bound states in continuum (BIC), EIT resonance

PACS: 73.21.–b, 73.63.–b, 73.20.At **DOI:** 10.1088/1674-1056/abad23

1. Introduction

In recent years, electron transport in a mesoscopic system has been a subject of intensive research.[1–3] Some mesoscopic quantum structures are able to exhibit important phenomena such as conductance quantization in ballistic transport,[4] Aharonov–Bohm (AB) effects,[5,6] Fano resonances,[7–10] and bound in continuum (BIC) states.[11–14] The BIC states are non-radiating, characterized by the resonant frequencies embedded in the continuum spectrum of radiating modes of the surrounding space, whereas Fano resonance is a kind of resonance followed by an anti-resonance and is characterized by an asymmetric line profile. In the literature, there are many different geometries of mesoscopic structures in which the Fano resonance has been explored and studied. Among these geometries, the AB ring made of two arms with a quantum dot (QD) embedded in one arm has been studied and analyzed experimentally and theoretically.[15–21] Also, different devices with different quantum dots have been discussed in several studies.[13,14,22,23] Recently, the interest in these phenomena has been strengthened by some of us in two connected mesoscopic AB rings.[24]

In addition to Fano resonances, electromagnetically induced transparency (EIT) resonances have attracted enormous attention due to their interesting physics and potential applications such as slow light effect and data storage.[25] This phenomenon refers to the coherent interactions between the excitation pathways to the atomic upper levels,[26,27] which can lead to a sharp narrowband transparency window within a broad absorption spectrum.[28,29] In condensed matter physics, the analogue of BIC, Fano, and EIT phenomena have been demonstrated in different types of structures, such as photonic crystal cavities,[30] metamaterials,[31–38] acoustic waveguides,[39] solid–liquid multilayers,[40] and photonic circuits.[41,42]

In the literature, several studies dealing with transmission zeros in stubbed structures have been reported in relation with Fano and EIT resonances in various mesoscopic waveguide systems.[43–45] Some years ago,[46] we studied symmetric and asymmetric Fano resonances[6] in a loop structure with two stubs grafted on both sides. Recently,[47] we have investigated the EIT resonances and BIC states in a simple mesoscopic structure made of double Aharonov–Bohm rings. This structure may exhibit a transmission gap and an EIT resonance in a transmission spectrum without inserting any perturbation in the arms of the rings; in particular we have shown that the shape of the EIT resonance and the width of the transmission dip can be tailored by varying the magnetic flux threading the rings as well as the geometry of the structure. In another recent work,[48] we have proposed a simple mesoscopic quantum structure that can give rise to BIC states. These states, which appear as hidden resonances with infinite lifetime, can be transformed into EIT and EIR (electromagnetic induced reflection) resonances by means of the magnetic flux. In this work, EIT and EIR resonances are analyzed as a function of magnetic flux threading the loop as well as temperature. Also, the Fano parameter q and the quality factor Q for each of these resonances have been deduced and analyzed as a function of

†Corresponding author. E-mail: t.mrabti@yahoo.fr

© 2020 Chinese Physical Society and IOP Publishing Ltd

magnetic flux.

In this paper, we study a simple mesoscopic demultiplexer device by using induced transparency resonances. The objective of this work is twofold. (i) We propose a simple mesoscopic structure (Fig. 1(a)) composed of two waveguide resonators (stubs) grafted on the same site. This structure can support trapped states (also called BIC states[11]) for specific values of the resonators lengths (d_1 and d_2): these trapped states can be transformed into EIT resonances by detuning appropriately d_1 and d_2. (ii) The cross structure is then proposed to realize a mesoscopic demultiplexer with an input waveguide and two output waveguides (Fig. 1(b)) where a specific cross structure is placed on each waveguide, namely two resonators of lengths d_1 and d_2 are inserted along the first waveguide at a distance d_5 from the input waveguide, while the second waveguide is composed of two resonators of lengths d_3 and d_4, which are separated from the input by a wire of length d_6. Because of the existence of transmission zero around the EIT resonance, we obtain the closed form expressions of the geometrical parameters that enable the deducing of a perfect transfer of a given state in the first waveguide without perturbing the second waveguide. Also, we analyze the effect of the temperature on the resonance in the conductance spectrum by using Landauer–Büttiker formula. The theoretical results are obtained using the Green's function approach.[49] This method of calculation enables the deducing of dispersion relations as well as transmission and reflection coefficients. It is worth mentioning that in two recent papers,[50,51] we have demonstrated the possibility to realize magnonic and photonic demultiplexer circuits based on the EIT resonances. Each of these systems consists of an input waveguide and two output waveguides in Y-shape. Also, an electron multiplexer composed of two semiconductor quantum wires resonantly coupled has been proposed.[52,53] This add–drop system enables a good selectivity of the directional transfer of electrons from one line to another line.

The rest of this paper is organized as follows. In Section 2, we present some steps of the Green's function which enables the calculating of the transmission and reflection coefficients in the cross structure. Then, we show in Section 3 how one can deduce analytically and numerically BIC states as well as EIT resonances. In Section 4 we give analytical and numerical results about the possibility to realize perfect demultiplexing in a Y-shaped structure by using EIT resonance. The effect of temperature on such a resonance is also highlighted. The main conclusions of this work are given in Section 5.

2. Theoretical model: the Green's function approach

The electronic transport in the mesoscopic structure presented in this work is performed within the framework of the interface response theory of continuous media.[49] The objective of this theory is to calculate the Green's function of a composite system containing a large number of interfaces that separate different homogenous media. The present theory allows us to perform the calculations of reflection and transmission coefficients as well as the dispersion relations. All the matrix elements $g(DD)$ in the whole space D of the composite material, can be obtained from the knowledge of the matrix elements $g(MM)$ in the interface space M. The $g(MM)$ is calculated from its inverse $g^{-1}(MM)$. The latter is formed by a linear superposition of the surface matrix elements $g_i^{-1}(MM)$ of any independent wire bounded by perfectly free interfaces with appropriate boundary conditions.[49]

Hence, before treating the whole structure, it would be useful to know the Green surface elements of its elementary constituents, namely, the Green's function of a finite resonator of length d_i ($i = 1, 2$) and semi-infinite leads. The Schrödinger equation describing the motion of an electron in a potential barrier $V_i(x)$ is given by

$$\frac{-\hbar^2}{2m}\left\{\frac{\mathrm{d}^2}{\mathrm{d}x^2}+V_i(x)\right\}\psi(x)=E\psi(x), \tag{1}$$

where x is the coordinate along the quantum wire, $\hbar$ is the reduced Planck constant, and m is the effective mass of the electron. For the present case, neither potential barrier nor impurity exists in the system, namely $V_i(x)=0$. The corresponding Green's function between two points x and x' is defined by

$$-\frac{\hbar^2}{2m}\left\{\frac{\mathrm{d}^2}{\mathrm{d}x^2}-\alpha^2\right\}G(x,x')=\delta(x-x'), \tag{2}$$

where $\alpha=-\mathrm{j}k$, $\mathrm{j}=\sqrt{-1}$, and $k=\sqrt{2mE}/\hbar$, with k being the wave vector. The solution of Eq. (2) is given by

$$G(x,x')=\frac{\mathrm{j}}{2F}\mathrm{e}^{\mathrm{j}k(x-x')}, \tag{3}$$

where $F=(\hbar^2/2m)k$. From Eq. (3) one can easily calculate[54] the Green function of a finite resonator of length d_i ($i = 1, 2$) in the space of its interface $M=\{0,d_i\}$ and then deduce the inverse g_r^{-1} of this (2×2) matrix as follows:

$$g_{\mathrm{r}}^{-1}=-F\begin{pmatrix} C_i/S_i & -1/S_i \\ -1/S_i & C_i/S_i \end{pmatrix}, \tag{4}$$

where $S_i=\sin(kd_i)$, and $C_i=\cos(kd_i)$ ($i = 1, 2$).

The inverse of the Green's function of semi-infinite lead can be written as

$$g_{\mathrm{s}}^{-1}(M,M)=-\mathrm{j}F. \tag{5}$$

3. BIC states and EIT resonances in a cross quantum structure

The mesoscopic structure presented in Fig. 1(a) consists of two resonators characterized by their lengths d_1 and d_2 and

inserted at the same place along an infinite quantum waveguide. Each resonator induces its own transmission to be zero, whereas the resonator of length $d = d_1 + d_2$ induces a complete transmission resonance between the two transmission zeros.

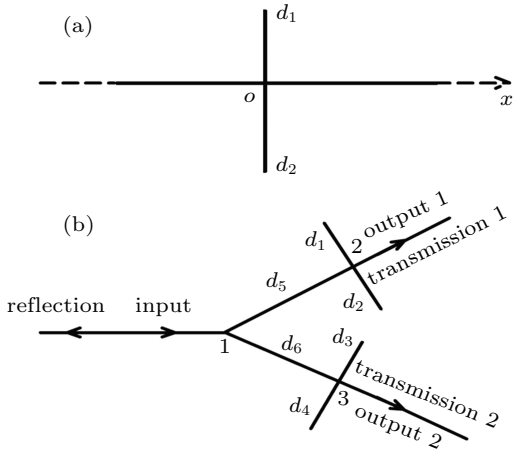


Fig. 1. (a) Schematic illustration of one-dimensional mesoscopic system with two grafted resonators of lengths d_1 and d_2 on the same site. The whole structure is inserted between two semi-infinite leads. (b) Schematic representation of a mesoscopic demultiplexer device with one input waveguide and two output waveguides.Two resonators of lengths d_1 and d_2 are inserted along the first waveguide at distance d_5 from the input waveguide, whereas the second waveguide is composed of two resonators of lengths d_3 and d_4 separated from the input by a wire of length d_6.

In order to understand and analyze the behavior of the BIC phenomenon and EIT phenomenon presented by the cross structure, first we calculate the transmission (t) and reflection (r) coefficients by the Green's function method. To calculate t and r, we need first the Green's function element $g^{-1}(0,0)$ of the whole system (Fig. 1(a)) at the interface point $x = 0$. This quantity can be obtained from a superposition of the inverse of Green's function of the different components, namely two semi-infinite waveguides (Eq. (5)) and two resonators (Eq. (4)) of lengths d_1 and d_2, namely,[54]

$$g^{-1}(0,0) = -2\mathrm{j}F - \frac{FC_1}{S_1} - \frac{FC_2}{S_2}, \tag{6}$$

where $S_1 = \sin(kd_1)$, $C_1 = \cos(kd_1)$, $S_2 = \sin(kd_2)$, $C_2 = \cos(kd_2)$, $F = (\hbar^2/2m)k$, $\mathrm{j} = \sqrt{-1}$, and $k = \sqrt{2mE}/\hbar$ with $\hbar$, k, and m being respectively the reduced Planck constant, the wave vector, and the effective mass of the electron. By inverting again $g^{-1}(0,0)$, the transmission and reflection coefficient can be calculated from the equation[54] $t = -2\mathrm{j}Fg(0,0)$ or equivalently

$$t = \frac{2S_1S_2}{2S_1S_2 + \mathrm{j}S}. \tag{7}$$

Similarly, the reflection coefficient can be obtained from[54] $r = -1 - 2\mathrm{j}Fg(0,0)$ or equivalently

$$r = \frac{-\mathrm{j}S}{2S_1S_2 + \mathrm{j}S}, \tag{8}$$

where $S = \sin(kd)$ and $d = d_1 + d_2$. From the expressions of t (Eq. (7)) and r (Eq. (8)), one can deduce the transmission rate and reflection rate as $T = |t|^2$ and $R = |r|^2$. Then, one can check easily the conservation law $R + T = 1$.

As is well known, the eigenstates of the system can be obtained from the pole of the Green's function (Eq. (6)) or similarly the transmission coefficient (Eq. (6)), namely,

$$2S_1S_2 + \mathrm{j}S = 0. \tag{9}$$

This latter equation has the form of a complex quantity. Its real part gives the position of the resonance in the transmission coefficient, whereas its imaginary part is related to the width of the resonance. In general, it is not easy to simultaneously cancel real and imaginary part of Eq. (9) at the same energy. However, when this happens, it will correspond to a bound state falling in a continuum of states induced by the semi-infinite wires. Indeed, if the lengths d_1 and d_2 are chosen to be commensurate, then equation (9) can be factorized by a real term whose zeros give the BIC states. The factorization can take place if

$$d_1 = \frac{m_1}{m_1 + m_2} d_0, \tag{10}$$

$$d_2 = \frac{m_2}{m_1 + m_2} d_0, \tag{11}$$

where m_1 and m_2 are non-zero integers, then we obtain $S_1 = S_0\mathrm{U}_{m_1-1}(C_0)$, $S_2 = S_0\mathrm{U}_{m_2-1}(C_0)$, and $S = S_0\mathrm{U}_{m_1+m_2-1}(C_0)$ with

$$S_0 = \sin\left(\frac{kd_0}{m_1 + m_2}\right), \quad C_0 = \cos\left(\frac{kd_0}{m_1 + m_2}\right),$$

and $\mathrm{U}_m(x)$ being the Chebyshev polynomial of the second kind of degree m. Therefore, equation (9) can be factorized by the term S_0. Then, if $S_0 = 0$, one obtains the energy for each of the BIC states given by

$$kd_0 = n(m_1 + m_2)\pi, \tag{12}$$

where n is an no-zero integer.

In a particular case of similar resonators (*i.e.*, $m_1 = m_2 = 1$ and $d_1 = d_2 = 0.5d$), equation (9) can be factorized by the term S_1 as follows:

$$S_1(2S_1 + \mathrm{j}2C_1) = 0. \tag{13}$$

Equation (13) clearly shows that BIC states are given by

$$S_1 = 0, \tag{14}$$

or equivalently $kd_1 = n\pi$ (*i.e.*, $kd_0/2 = n\pi$; n is an integer, see Eq. (12)). Therefore, the first BIC state ($n = 1$) can be obtained from $kd = 2\pi$. In what follows, we shall give the reduced energy in terms of $\kappa = kd/\pi$. Figure 2(a) shows the curve of transmission *versus* κ for $d_1 = d_2 = d/2$. The vertical bar shows the position of the BIC state with zero width, and its position on the abscissa axis is denoted by a solid circle in Fig. 2(a).

In Fig. 2(b), the red and blue curves represent the transmission coefficients *versus* reduced wave vector κ for single resonators of lengths $d_1 = 0.55d$ and $d_2 = 0.45d_0$ respectively. The expressions giving the transmission and reflection coefficients for the latter systems, can be deduced from Eqs. (7) and (8) by cancelling one of the two resonators in Eqs. (7) and (8). We can remark that each resonator induces its own transmission zero given by $S_i = 0$ ($i = 1, 2$) (*i.e.*, $\kappa = 2.22$ for $d_1 = 0.45d$ and $\kappa = 1.82$ for $d_2 = 0.55d$). Now, when both resonators are grafted at the same time, we obtain the black curve in Fig. 2(b) where the two transmission zeros associated with each resonator fall at the same position of those of the resonators taken alone. In addition, we can clearly notice that the BIC state (hidden resonance) falling at $\kappa = 2$ (Fig. 2(a)) where the device behaves as an opaque system, is transformed into a resonance inserted between two transmission zeros where the device exhibits a transparency energy domain (full transmission). This is the result of a constructive interference between the two resonators, inducing the so-called EIT resonance. By varying the detuning length $\delta = d_2 - d_1$ between the two resonators, one can adjust the width Γ of the EIT resonance. In particular when δ decreases, Γ decreases and collapses for $\delta = 0$ (*i.e.* $d_1 = d_2$), reducing to a hidden resonance or a BIC state[11] with an infinite quality factor (*i.e.*, infinite lifetime) as shown in Fig. 2(a). This is a stationary wavefunction in the two resonators with a node at the connecting waveguide. Therefore, such a state does not interact with the continuum states associated to the infinite quantum wire that can transport energy away (see below). In this case, the system becomes opaque (Fig. 2(a)), giving rise to a complete reflection of the wave function corresponding to $\kappa = 2$.

It is noteworthy that some years ago, Tan *et al.*[55] proposed an acoustic structure composed of two dangling Helmholtz acoustic resonators located at the same axial position. They have shown experimentally and numerically the existence of EIT resonance, mimicking thereby the quantum interference between two direct excitation pathways in a three level V-type atom. Our system is analogous to this system but for a quantum waveguide. In the insets of Figs. 2(a), we give a schematic representation of the three energy levels. The level is associated with the ground state of the continuum states in the waveguide, whereas **1** and **2** indicate the two energy levels induced by the two stubs. In Fig. 2(a), the two stubs are similar, giving rise to two degeneracy states $\mathbf{1} = \mathbf{2}$, and the shrinking of the resonance lying between them. Here the system is opaque as no filtered resonance exists. However, in Fig. 2(b), the two stubs are slightly different, therefore the degeneracy is lifted between the two levels $\mathbf{1} \neq \mathbf{2}$, giving rise to a transparency window between them (Fig. 2(b)).

The behavior of the square modulus of the wave-function in the structure is given in Fig. 3 for the BIC state at $\kappa = 2$ and $d_1 = d_2 = 0.5d_0$ (Fig. 2(a)) and for the EIT resonance at $\kappa = 2$ and $d_1 = 0.4d_0$ and $d_2 = 0.6d_0$ (Fig. 2(b)). In the case of the BIC state (Fig. 3(a)) as predicted, the wave-function does not propagate on the right side of the waveguide (transmission zero). Indeed, $\kappa = 2$ corresponds exactly to the eigenstates of the two identical stubs with vanishing wave-function on both sides, so the incident wave interacts destructively with the wave-function in the stubs and is totally reflected. At the same time there is an additional state of the whole vertical segment which has a node at the connection point with the horizontal waveguide. This latter state is not affected by the incident wave which confers on it the characteristic of a BIC state as mentioned in Fig. 2(a). When the lengths d_1 and d_2 are slightly detuned from $d_0/2$, the energy values of transmission zeros are shifted from the BIC state. At the same time the node of the latter state happens at a different position from the connection point with the horizontal waveguide (see Fig. 3(b)) and allows it to interact with the incident wave, thus revealing the BIC state as an EIT peak in the transmission spectrum (Fig. 2(b)).

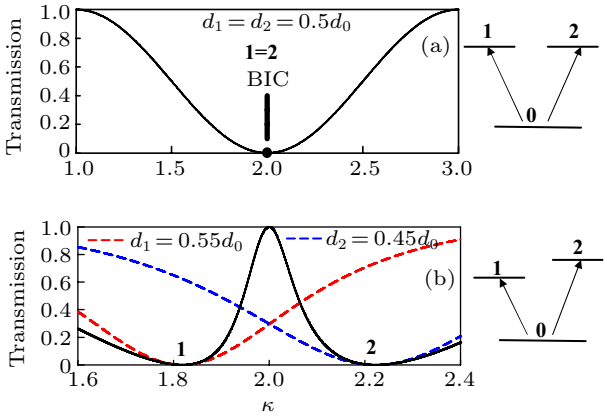


Fig. 2. Curve of transmission coefficient *versus* dimensionless wavevector κ. (a) Two grafted resonators are considered to be similar, *i.e.*, $d_1 = d_2 = 0.5d$. (b) Red (blue) curve corresponds to transmission through a single resonator of length $d_1 = 0.55d$ ($d_2 = 0.45d$) along waveguide. Black curve corresponds to the case when the two resonators are placed together at the same point. Insets in panels (a) and (b) show the analogy to a three-level V-type atom, with degenerate $\mathbf{1} = \mathbf{2}$ and nondegenerate $\mathbf{1} \neq \mathbf{2}$ energy levels, respectively.

In order to confirm that the obtained resonance presents indeed an EIT shape, we perform a Taylor expansion of the transmission rate (Eq. (7)) around the resonance at $\kappa = 2$ (*i.e.* $kd = 2\pi + \varepsilon$). After some straightforward calculations, the transmission rate T can be written below following a Fano shape

$$T = A\frac{(\varepsilon+q_1\Gamma)^2(\varepsilon-q_2\Gamma)^2}{\varepsilon(\varepsilon+\beta)+\Gamma^2}, \tag{15}$$

where $A = 4\pi^2\alpha\alpha'/(4\Delta^4+\pi^2)$, $\beta = 8\pi\Delta^4/(4\Delta^4+\pi^2)$, $\alpha = \Delta/2\pi+1/2$, $\alpha' = 1/2-\Delta/2\pi$, $\Delta = 2\pi(d_1/d_0-1/2)$, and

$$\Gamma = \frac{2\pi\Delta^2}{\sqrt{4\Delta^4+\pi^2}} \tag{16}$$

is the full width at half maximum of the EIT resonance falling at $\varepsilon = 0$ (*i.e.*, $\kappa = 2$). The two quantities $q_1 = \sqrt{4\Delta^4+\pi^2}/4\alpha\pi\Delta$ and $q_2 = \sqrt{4\Delta^4+\pi^2}/4\alpha'\pi\Delta$ are the Fano parameters; they represent qualitatively the magnitude of the interference between the bound state and the propagating continuum state.[56,57] One can notice that Γ increases (*i.e.*, the quality factor decreases) and q_1 and q_2 decrease as δ increases.

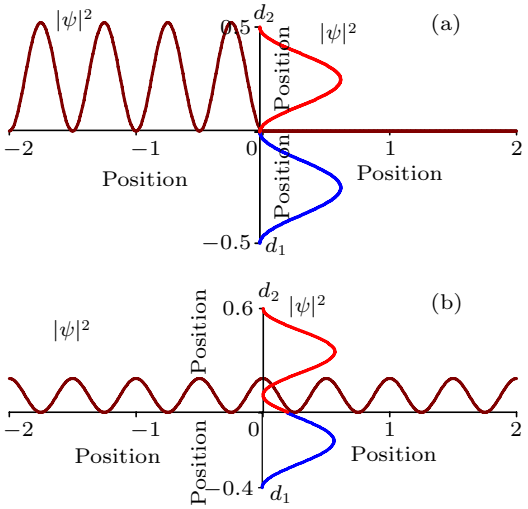


Fig. 3. Square modulus of wave-function as a function of space position (in units of d_0) in structure for $\kappa = 2$ and (a) $d_1 = d_2 = 0.5d_0$ and (b) $d_1 = 0.4d_0$ and $d_2 = 0.6d_0$.

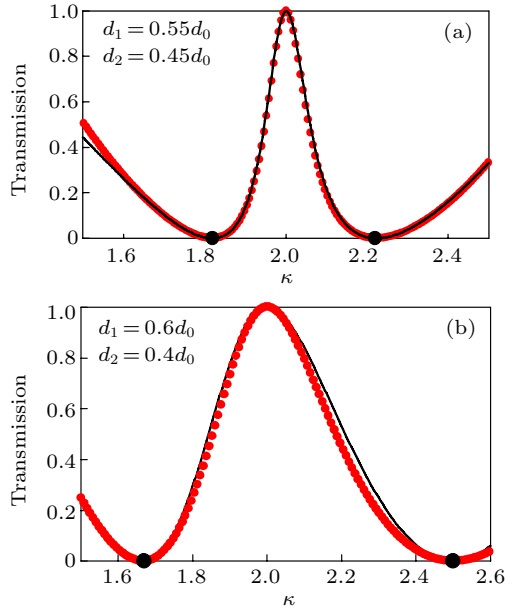


Fig. 4. Transmission spectra as a function of reduced wavevector κ. Exact (full line) and approximate results (red circles) obtained by Taylor expansion (Eq. (15)) are sketched around the EIT resonance. The two resonators' lengths are (a) $d_1 = 0.55d$ and $d_2 = 0.45d$, and (b) $d_1 = 0.6d$ and $d_2 = 0.4d$.

The results of the approximate expression (Eq. (15)) are represented by red circles in Fig. 4 for two values of δ : $\delta = 0.1d$ (Fig. 4(a)) and $\delta = 0.2d$ (Fig. 4(b)). These two curves clearly show that the resonance presents an EIT shape with $q_1 = 1.45$, $q_2 = 1.77$, and width $2\Gamma = 0.4$ in the case of $\delta = 0.1d$ (Fig. 4(a)). This induced resonance is trapped between two transmission zeroes, indicated by solid circles on the abscissa axis around $\kappa = 2$ in Fig. 4, and reaches unity (*i.e.* $T = 1$) for a lossless system. However, the above calculation shows that a well-defined EIT resonance with a width 2Γ and coupling parameters q_1 and q_2 can be found. These latter quantities can be fixed by varying the lengths of the two resonators (*i.e.*, δ). The curves show very good agreement between the exact calculation (black curves) and the approximate one derived from a Taylor expansion (red circles) of the transmission at the vicinity of the resonance energy.

4. Quantum demultiplexer device using induced resonances

4.1. Analytical results

The schematic illustration of the demultiplexer device is shown in Fig. 1(b). It consists of an input waveguide and two output waveguides with a Y shape. Along the first waveguide, two resonators of lengths d_1 and d_2 are placed at the site marked as 2 at a distance d_5 from the input connector marked as 1. Similarly, along the second waveguide, two resonators of lengths d_3 and d_4 are placed at the site marked as 3 at a distance d_6 from the input connector 1. Using the Green's function method, we can obtain the expressions of transmission and reflection coefficients in the closed form. To do so, we need to inverse the Green's function $g^{-1}(M,M)$ in the interface space $M = \{1,2,3\}$ of the whole system (Fig. 1(b)). This quantity can be obtained from a superposition of the inverse Green's function of its elementary constituents as shown below.

(i) The inverse of the surface Green's function element of the three semi-infinite waveguides (see Eq. (5)) at entrance 1 and exits 2 and 3[54] is

$$g_s^{-1}(1,1) = g_s^{-1}(2,2) = g_s^{-1}(3,3) = -\mathrm{j}F. \tag{16a}$$

(ii) The inverse of the surface Green's functions of the stubs placed at the site $\{2\}$ and the site $\{3\}$ are[54]

$$g_i^{-1}(2,2) = g_i^{-1}(3,3) = -F_i\frac{C_i}{S_i} \quad (i = 1,2,3,4). \tag{16b}$$

(iii) The inverse of the surface Green's functions of the waveguides of lengths d_5 and d_6 (see Eq. (4)) in the space of interfaces $M_5 = \{1,2\}$ and $M_6 = \{1,3\}$ respectively (Fig. 1(b)) are[54]

$$g_i^{-1}(M_i,M_i) = -F_i\begin{pmatrix} C_i/S_i & -1/S_i \\ -1/S_i & C_i/S_i \end{pmatrix} \quad (i = 5,6), \tag{16c}$$

where $C_i = \cos(kd_i)$, $S_i = \sin(kd_i)$ (i = 1, 2, 3, 4, 5, 6).

For simplicity, we assume that all the quantum waveguides are identical, *i.e.*, $F_i = F$ ($i = 1$–6) such as for GaAs semiconductor material. From Eqs. (16a)–(16c), one can construct the inverse of the Green's function $g^{-1}(M,M)$ of the whole system (Fig. 1(b)) in the interface space $M = \{1,2,3\}$. This quantity is obtained just from a linear superposition of the preceding constituents, namely,

$$g^{-1}(M,M) = -F \begin{pmatrix} \mathrm{j} + C_5/S_5 + C_6/S_6 & -1/S_5 & -1/S_6 \\ -1/S_5 & C_5/S_5 + C_1/S_1 + C_2/S_2 + \mathrm{j} & 0 \\ -1/S_6 & 0 & \mathrm{j} + C_3/S_3 + C_4/S_4 + C_6/S_6 \end{pmatrix}. \tag{17}$$

The reflection coefficient in the input waveguide of the demultiplexer can be obtained from the equation[54] $r = -1 - 2\mathrm{j}Fg(0,0)$. After some algebraic calculations, one obtains

$$r = -\frac{\varepsilon_1 + \mathrm{j}\varepsilon_2}{\chi_1 + \mathrm{j}\chi_2}, \tag{18}$$

where

$$\begin{aligned} \varepsilon_1 &= S_1S_2S_3S_4(S_5S_6 - C_5C_6) - S_1S_2S'C_6S_5 \\ &\quad - S_3S_4SC_5S_6 + SS'S_5S_6, \end{aligned} \tag{19}$$

$$\begin{aligned} \varepsilon_2 &= S_1S_2S_3S_4(C_5S_6 + C_6S_5) - S_1S_2S'C_6C_5 \\ &\quad - S_3S_4SC_5S_6 - SS'S_0, \end{aligned} \tag{20}$$

$$\begin{aligned} \chi_1 &= 3S_1S_2S_3S_4(S_5S_6 - C_5C_6) - S_1S_2S'(C_5S_6 + S_0) \\ &\quad - S_3S_4S(C_6S_5 + S_0) - SS'S_5, \end{aligned} \tag{21}$$

$$\begin{aligned} \chi_2 &= 3S_1S_2S_3S_4(C_5S_6 + C_6S_5) + S_1S_2S'(2S_5S_6 - C_5C_6) \\ &\quad + S_3S_4S(2S_6S_5 - C_5C_6) - S_0S'S, \end{aligned} \tag{22}$$

and $S = \sin(k(d_5 + d_6))$, $S = \sin(k(d_1 + d_2))$, $S' = \sin(k(d_3 + d_4))$.

Similarly, the amplitudes of the transmitted waves in the two output waveguides (Fig. 1(b)) are given respectively by the equations[48] $t_1 = -2\mathrm{j}Fg(1,2)$ and $t_2 = -2\mathrm{j}Fg(1,3)$. After some algebraic calculations, one obtains

$$t_1 = \frac{2S_1S_2(-C_6S_3S_4 - S'S_6 + \mathrm{j}S_3S_4S_6)}{\chi_1 + \mathrm{j}\chi_2}, \tag{23}$$

$$t_2 = \frac{2S_3S_4(-C_5S_1S_2 - SS_5 + \mathrm{j}S_1S_2S_5)}{\chi_1 + \mathrm{j}\chi_2}. \tag{24}$$

The expression of reflection rate R in the input waveguide is given by $R = |r|^2$, while the transmission coefficients in the two output waveguides are given respectively by $T_1 = |t_1|^2$ and $T_2 = |t_2|^2$. From the expressions of reflection and transmission coefficient rates, one can check the energy conservation, namely $T_1 + T_2 + R = 1$.

4.2. Numerical results of demultiplexing phenomenon based on EIT resonance

Now we are looking for the necessary conditions to obtain a total transmission in one output waveguide without disturbing the other waveguide: these conditions can be obtained as a function of geometrical parameters of the structure for a given value of reduced wavevector κ. Indeed, in order to achieve $|T_1| = 1$, $T_2 = 0$, and $R = 0$ in the first waveguide, one can show easily from Eqs. (18), (23), and (24) that the following conditions should be satisfied: $S_3S_4 = 0$ (*i.e.*, $S_3 = 0$ or $S_4 = 0$), $S = 0$ and $C_6 = 0$. Similarly, in order to achieve $|T_2| = 1$, $T_1 = 0$, and $R = 0$ in the second output waveguide, the following conditions should be satisfied: $S_1S_2 = 0$, $S' = 0$ and $C_5 = 0$.

From the above conditions, one can deduce the necessary conditions that should be satisfied by the six lengths of the finite waveguides d_1, d_2, d_3, d_4, d_5, and d_6 in order to realize perfect demultiplexing, namely,

$$d_3 = \frac{d_1 + d_2}{2}, \tag{25}$$

$$d_4 = \frac{3d_2 - d_1}{2}, \tag{26}$$

$$d_5 = \frac{d_2}{2}, \tag{27}$$

$$d_6 = \frac{d_3}{2} = \frac{d_1 + d_2}{4}. \tag{28}$$

The above expressions can be rewritten also as a function of detuning $\delta = d_2 - d_1$ between resonators 1 and 2 as well as the total length of these resonators (*i.e.*, $d = d_1 + d_2$). Indeed, as mentioned analytically in Section 2, fixing the values of length d_0 for the two resonators 1 and 2 can fix the position of the EIT resonance along the output 1, then by taking the lengths of the two resonators to be slightly different (*i.e.*, $\delta \approx 0$), the conditions described previously in Eqs. (25)–(28), become respectively

$$d_1 = \frac{d_0}{2} - \frac{\delta}{2}, \tag{29}$$

$$d_2 = \frac{d_0}{2} + \frac{\delta}{2}, \tag{30}$$

$$d_3 = \frac{d_0}{2}, \tag{31}$$

$$d_4 = \frac{d_0}{2} + \delta, \tag{32}$$

$$d_5 = \frac{d_0}{4} + \frac{\delta}{4}, \tag{33}$$

$$d_6 = \frac{d_0}{4}. \tag{34}$$

In order to give a better insight into the analytical results presented above, we plot in Fig. 5 the curves of numerical results of the transmission spectra T_1 and T_2 along the first and second output waveguide as well as the curves of reflection spectrum R in the input waveguide *versus* the dimensionless wave vector κ for four values of δ around $\delta = 0$.

For $\delta = 0.15$ (Fig. 5(a)), we can see that when the transmission T_1 in the first output waveguide (red curve) reaches unity (*i.e.*, $T_1 = 1$), the reflection R (black curve) in the input waveguide and the transmission T_2 in the second output waveguide (blue curve) vanish (*i.e.*, $R = T_2 = 0$) . In addition, when the transmission spectrum in the second output waveguide (blue curve) reaches unity ($T_2 = 1$), the reflection R (black curve) in the input waveguide and the transmission T_1 in the first output waveguide (red curve) vanish (*i.e.*, $R = T_1 = 0$) . For $\delta = 0.1$ (Fig. 5(b)), we obtain the same results as those in Fig. 5(a), however as predicted, the width of EIT resonances become narrower. For $\delta = 0$ (Fig. 5(c)), all resonators 1, 2, 3 and 4 become similar. Therefore, both EIT resonances fall at the same energy (*i.e.*, $\kappa = 2$), the corresponding widths vanish, giving rise to confined BIC states in the lateral stubs. For $\delta < 0$ (Figs. 5(d) and 5(e)), we obtain the same results as those in Figs. 5(a) and 5(b), but this time the resonance in the second waveguide (blue curve) falls above the one in the first waveguide (red curve). These results show that depending on the sign of δ, the EIT resonance in the second line can fall below or above the EIT resonance in the first line.

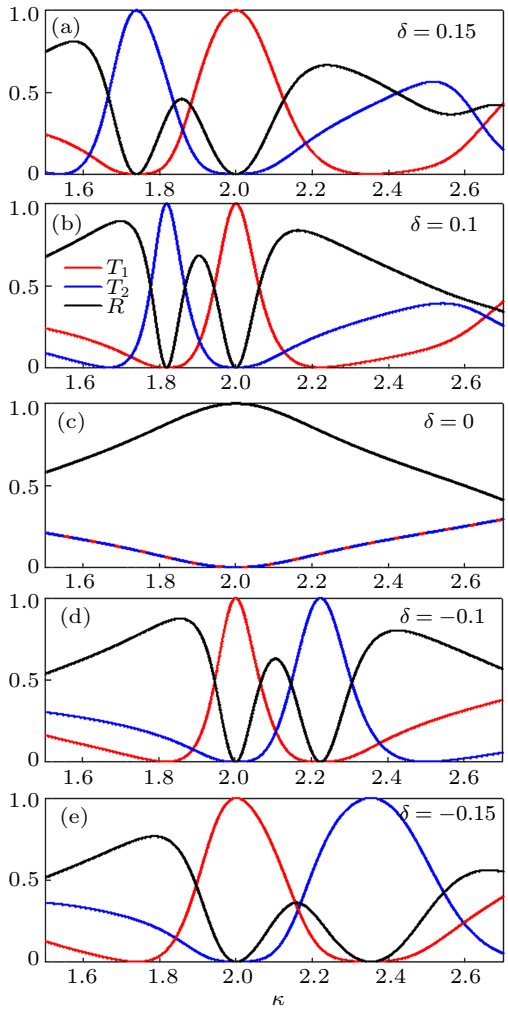


Fig. 5. Curves of transmission coefficient in output 1 (red curve) and output 2 (blue curve), and the reflected signal in the input of the demultiplexer device (black curve) *versus* dimensionless wavevector κ for five values of δ: $d_2 - d_1$, with $d = d_1 + d_2$ being fixed.

Indeed, as shown in Section 2, for a fixed d, the EIT resonance in one waveguide with two stubs, falls at the same reduced wave vector $\kappa = 2$ whatever the value of δ is. As δ decreases, the width of the EIT resonance decreases and vanishes for $\delta = 0$ (Fig. 2(a)). In the presence of the second output waveguide, the position and the width of the second EIT resonance depend strongly on the sign of δ (*i.e.*, when permuting the two resonators 1 and 2). Indeed, as the first EIT resonance exhibits two transmission zeros around $\kappa = 2$, the position of the second EIT resonance falls below $\kappa = 2$ for $\delta > 0$ on the left-hand side zero of the first EIT resonance. For $\delta = 0$, both resonances cross each other and for $\delta < 0$ the second EIT resonance reappears above $\kappa = 2$ on the right-hand side zero of the first EIT resonance (see Fig. 5).

4.3. Effect of temperature on transmission resonance

In this section, we are interested in the effect of temperature (θ) on transmission resonance. It should be noted that in all the results obtained in Subsection 4.2, we have not considered the thermal effect (*i.e.*, $\theta = 0$). By using the Landauer–Büttiker formula,[58,59] the conduction at a finite temperature of the transmission rate in one-dimensional channel can then be written as[2,3]

$$G_{\mathrm{T}}(E_{\mathrm{F}},\theta) = G_0 \int \mathrm{d}E \left(-\frac{\partial f(E,E_{\mathrm{F}},\theta)}{\partial E} \right) T(E), \quad (35)$$

where $G_0 = 2e^2/h$ is the quantum conductance, h the Planck constant, and $f(E)$ the Fermi distribution function given by $f(E,E_{\mathrm{F}},\theta) = [\mathrm{e}^{(E-E_{\mathrm{F}})/k_{\mathrm{B}}\theta} + 1]^{-1}$ with E_{F} being the Fermi energy and k_{B} being the Boltzmann constant. We change the variable from E to κ in the integral by using $E = E^*\kappa^2$ where $E^* = \hbar^2\pi^2/2md_0^2$. Also, we define a dimensionless temperature $\theta_{\mathrm{d}} = k_{\mathrm{B}}\theta/E^*$, then equation (35) can be written in the following form:

$$G_{\mathrm{T}}(\kappa_{\mathrm{F}},\theta) = \frac{G_0}{2\theta_{\mathrm{d}}} \int \mathrm{d}\kappa T(\kappa) \cosh^{-2}\left(\frac{\kappa^2 - \kappa_{\mathrm{F}}^2}{2\theta_{\mathrm{d}}} \right). \quad (36)$$

It is worth mentioning that equation (36) has been used to analyze the thermal effect on the Fano resonance in electronic transport of a quantum Aharonov–Bohm ring.[60–62] In the case that a GaAs mesoscopic structure with the length d_0 of the resonators (stubs) on the order of ~ 1 μm with effective electron mass $m = 0.067m_0$ (m_0 is the free electron mass) is really realized, a dimensionless temperature $\theta_{\mathrm{d}} = 0.1$ will correspond to $\theta = 6.5$ mK. These parameters are on the order of those presented in the experimental realization.[1,63–65]

In Figs. 6(a)–6(c), we plot the normalized conductance G_{T}/G as a function of dimensionless Fermi wave vector $\kappa_{\mathrm{F}} = (E_{\mathrm{F}} - E^*)^{1/2}$ for $\delta = 0.1$ and several values of the parameter θ_{d}. We note that the resonances in the conductances G_{T1} (red curve) and G_{T2} (blue curve) are very sensitive to the effect of temperature. Especially, when increasing the temperature, the

conductances G_{T1} and G_{T2} become broader and the amplitude of the conductance G_{T2} decreases more rapidly than the amplitude of the conductance G_{T1}. This is due to the fact that the width of the resonance along the second output is thinner than that of the resonance along the first output. The evolutions of the normalized conductance as a function of temperature θ_d and reduced wave-vector κ are provided in Figs. 7(a) and 7(b). We can notice that with temperature (θ_d) increasing from 0 to 0.1, the conductance G_{T1} around $\kappa = 2$ (Fig. 7(a)) and the conductance G_{T2} around $\kappa = 1.8$ (Fig. 7(b)) are considerably affected for $\theta_d > 0.08$ and $\theta_d > 0.06$ respectively. Note that the conductance is represented by color scale in Fig. 7.

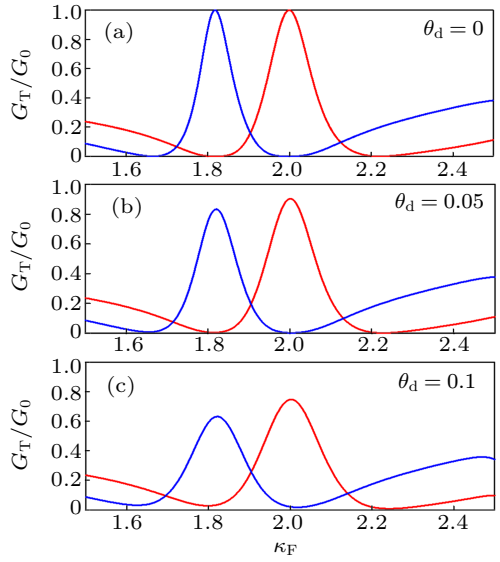


Fig. 6. Plots of normalized conductance *versus* dimensionless Fermi wave vector κ_F for $\delta = 0.1$ and different temperatures, with red color and blue color referring to outputs 1 and 2 respectively.

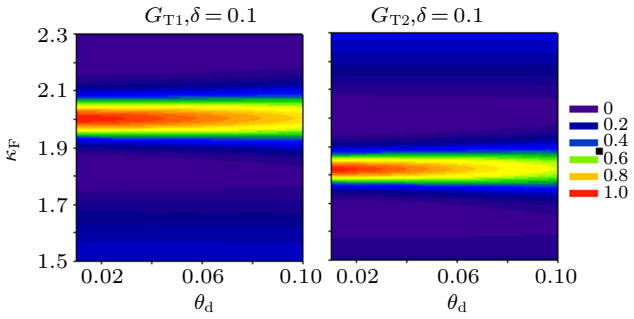


Fig. 7. Normalized conductance (in color scale) *versus* wave vector κ and temperature θ_d along the (a) first output and (b) second output for $\delta = 0.1$.

5. Conclusions

In this paper, we study analytically and numerically the possibility of existence of BIC state and EIT resonance in a simple mesoscopic structure made of two stubs of lengths d_1 and d_2 inserted at the same position along a quantum waveguide. The EIT resonance in the transmission spectrum can be tailored by detuning the lengths of the two resonators (*i.e.*, $\delta = d_2 - d_1$). From a Taylor expansion of the transmission rate T around the EIT resonance energy, we deduce the expression of T following a Fano form, which enables us to deduce the width, the position and the Fano parameters of the EIT resonance. Finally, we propose a simple mesoscopic device based on the EIT resonance. The idea is to make the energy of the EIT resonance in one line coincide with the transmission zero in the other line and the reflection zero in the input line. This property enables us to derive the analytical expression of the waveguide length of the demultiplexer to achieve a selective transfer of a single propagating state through one line without perturbing the other line. We show that the different lengths of the finite waveguide constituting the demultiplexer should be chosen appropriately in order to realize a perfect demultiplexing. In addition, the position and width (quality factor) of the selected resonance in each line depend strongly on the detuning δ between the lateral stubs in Fig. 1(b). Also, we analyze the temperature dependence of the resonance in the conductance by using Landauer–Büttiker formalism. We show that the increasing of temperature affects the shape of the conductance resonance, in particular, its amplitude and width change considerably.

We would like to note that throughout this paper, we restrict ourselves to the discussion and study of one-dimensional model. The one-dimensional quantum wire case provides a good approximation to a real wire with finite width at low temperatures at which only the lowest subband is filled,[66] which means that the wire behaves like a monomode waveguide. At higher temperatures, in the study of the conductance of the quantum waveguide, the two and three-dimensional model[67–69] and the Landauer–Büttiker formula should be used.[58,59] However, in the literature, several one-dimensional quantum models[70] have been proposed and studied theoretically[46,71] and experimentally.[63,64]

References

[1] Beenakker C W J and van Houten H 1991 *Solid State Phys.* **44** 1
[2] Datta S 1995 *Electronic Transport in Mesoscopic Systems* (Cambridge: Cambridge University Press)
[3] Imry Y 2001 *Introduction to Mesoscopic Physics* (Oxford: Oxford University Press)
[4] Li S, Huang G Y, Guo J K, Kang N, Caroff P and Xu H Q 2017 *Chin. Phys. B* **26** 027305
[5] Pedersen S, Hansen A E, Kristensen A, S?rensen C B and Lindelof P E 2000 *Phys. Rev. B* **61** 5457
[6] Liu J, Gao W X, Ismail K, Lee K Y, Hong J M and Washburn S 1993 *Phys. Rev. B* **48** 15148
[7] Fano U 1961 *Phys. Rev.* **124** 1866
[8] Voo K K and S C Chon 2005 *Phys. Rev. B* **72** 165307
[9] Wang X Q, Zhang S F, Jiang C, Yi G Y and Gong W J 2018 *Physica E* **104** 1
[10] Zhang C X, Ding X H, Wang R, Zhou Y Q and Kong L M 2012 *Chin. Phys. B* **21** 034202
[11] Hsu C W, Zhen B, Stone A D, Joannopoulos J D and Soljacic M 2016 *Nat. Rev. Mater.* **1** 16048
[12] Nakamura H, Hatano N, Garmon S and Petroky T 2007 *Phys. Rev. Lett.* **99** 210404
[13] Ladrón de Guevara M L, Claro F and Orellana P A 2003 *Phys. Rev. B* **67** 195335
[14] Moiseyev N 2009 *Phys. Rev. Lett.* **102** 167404

[15] Kobayashi K, Aikawa H, Katsumoto S and Iye Y 2002 *Phys. Rev. Lett.* **88** 256806
[16] Kobayashi K, Aikawa H, Katsumoto S and Iye Y 2003 *Phys. Rev. B* **68** 235304
[17] Benjamin C and Jayannavar A.M 2003 *Phys. Rev. B* **68** 085325
[18] Kobayashi K, Aikawa H, Sano A, Katsumoto S and Iye Y 2004 *Phys. Rev. B* **70** 035319
[19] Johnson A C, Marcus C M, Hanson M P and Gossard A C 2004 *Phys. Rev. Lett.* **93** 106803
[20] Gong W and Jiang C 2009 *J. Appl. Phys.* **106** 013710
[21] Nakanishi T and Terakura K 2004 *Phys. Rev. B* **69** 115307
[22] Ladrón de Guevara M L and Orellana P A 2006 *Phys. Rev. B* **73** 205303
[23] Lu H, Lü R and Zhu B F 2005 *Phys. Rev. B* **71** 235320
[24] Mrabti T, Labdouti Z, El Abouti O, El Boudouti E H, Fethi F and Djafari-Rouhani B 2018 *Phys. Lett. A* **382** 613
[25] Zhang S, Zhou S, Loy M M T, Wong G K L and Du S 2011 *Opt. Lett.* **36** 4530
[26] Boller K J, Imamoglu A and Harris S E 1991 *Phys. Rev. Lett.* **66** 20
[27] Harris S and Hau L 1999 *Phys. Rev. Lett.* **82** 4611
[28] Harris S E 1997 *Phys. Today* **50** 36
[29] Fleischhauer M, Imamoglu A and Marangos J P 2005 *Rev. Mod. Phys.* **77** 633
[30] Yang X, Yu M, Kwong D L and Wong C W 2009 *Phys. Rev. Lett.* **102** 173902
[31] Kurter C, Tassin P, Zhang L, Koschny T, Zhuravel A P, Ustinov A V, Anlage SM and Soukoulis C M 2011 *Phys. Rev. Lett.* **107** 043901
[32] Jung H, Jo H, Lee W, Kim B, Choi H, Kang M S and Lee H 2019 *Adv. Opt. Mater.* **7** 1801205
[33] Fan Y, Qiao T, Zhang F, Fu Q, Dong J, Kong B and Li H 2017 *Sci. Rep.* **7** 40441
[34] Manjappa M, Pitchappa P, Singh N, Wang N, Zheludev N I, Lee C and Singh R 2018 *Nat. Commun.* **9** 4056
[35] Han S, Rybin M V, Pitchappa P, Srivastava Y K, Kivshar Y S and Singh R 2019 *Adv. Opt. Mater.* **8** 1900959
[36] Han S, Cong L, Srivastava Y K, Qiang B, Rybin M V, Kumar A, Jain R, Lim W X, Achanta V G, Prabhu S S, Wang Q J, Kivshar Y S and Singh R 2019 *Adv. Mater.* **31** 1901921
[37] Cong L and Singh R 2019 *Adv. Opt. Mater.* **7** 1900383
[38] Tan T C W, Plum E and Singh R 2020 *Adv. Opt. Mater.* **8** 1901572
[39] Al-Wahsh H, El Boudouti E H, Djafari-Rouhani B, Akjouj A, Mrabti T and Dobrzynski L 2008 *Phys. Rev. B* **78** 075401
[40] Quotane I, El Boudouti E H and Djafari-Rouhani B 2018 *Phys. Rev. B* **97** 024304
[41] Mouadili A, El Boudouti E H, Soltani A, Talbi A, Akjouj A and Djafari-Rouhani B 2013 *J. Appl. Phys.* **113** 164101
[42] Mouadili A, El Boudouti E H, Soltani A, Talbi A, Djafari- Rouhani B, Akjouj A and Haddadi K 2014 *J. Phys.: Condens. Matter* **26** 505901
[43] Rotter I and Sadreev A F 2005 *Phys. Rev E* **71** 046204
[44] Porod W, Shao Z and Lent C S 1992 *Appl. Phys. Lett.* **61** 1350
[45] Shao Z, Porod W, and Lent C S 1993 *Phys. Rev. B* **49** 11
[46] Al-Wahsh H, El Boudouti E H, Djafari-Rouhani B, Akjouj A and Dobrzynski L 2007 *Phys. Rev. B* **75** 125313
[47] Mrabti T, Labdouti Z, El Boudouti E H, Fethi F, El Abouti O and Djafari-Rouhani B 2019 *Materials Today: Proceedings* **13** 1055
[48] Mrabti T, Labdouti Z, Mouadili A, El Boudouti E H and Djafari-Rouhanid B 2020 *Physica E* **116** 113770
[49] Dobrzynski L, El Boudouti E H, Akjouj A, Pennec Y, Al-Wahsh H, Levéque G and Djafari-Rouhani B 2017 *Phononics* (Elsevier)
[50] Mouadili A, El Boudouti E H, Soltani A, Talbi A, Haddadi K, Akjouj A and Djafari-Rouhani B 2019 *J. Phys. D Appl. Phys.* **52** 075101
[51] Mouadili A, El Boudouti E H, Akjouj A, Al-Wahsh H, Djafari-Rouhani B and Dobrzynski L 2019 *AIP Advances* **9** 035011
[52] Kucharczyk R, Dobrzynski L, Djafari-Rouhani B and Akjouj A 2004 *Physica E* **24** 355
[53] Dobrzynski L, Akjouj A, Djafari-Rouhani B, Vasseur J O, Bouazaoui M, Vilcot J P, Beaurain A and McMurtry S 2003 *Phys. Rev. E* **67** 057603
[54] Vasseur J O, Akjouj A, Dobrzynski L, Djafari-Rouhani B and El Boudouti E H 2004 *Surf. Sci. Rep.* **54** 1
[55] Tan W, Yang C Z, Liu H S, Wang Z G, Lin H Q and Chen H 2012 *EPL* **97** 24003
[56] Raymond Ooi C H and Kam C H 2010 *Phys. Rev. B* **81** 195119
[57] Li B B, Xiao Y F, Zou C L, Jiang X F, Liu Y C, Sun F W, Li Y and Gong Q 2012 *Appl. Phys. Lett.* **100** 021108
[58] Landauer R 1957 *IBM J. Res. Dev.* **1** 223
[59] Büttiker M 1988 *Phys. Rev. B* **38** 9375
[60] Cassé M, Kvon Z D, Gusev G M, Olshanetskii E B, Litvin L V, Plotnikov A V, Maude D K and Portal J C 2000 *Phys. Rev. B* **62** 2624
[61] Vargiamidis V and Polatoglou H M 2007 *Phys. Rev. B* **75** 153308
[62] Vargiamidis V and Polatoglou H M 2006 *Phys. Rev. B* **74** 235323
[63] Mark A R, and Wiley P K 1989 *Nanostructure Physics and Fabrication* (London: Academic Press, Inc. LTD)
[64] International Symposium, College Station, Texas, March 13–15, p. 165
[65] Kouwenhoven L P, Hekking F W J, van Wees B J, Harmans C J P M, Timmering C E and Foxon C T 1990 *Phys. Rev. Lett.* **65** 361
[66] Deo P S and Jayannavar A M 1994 *Phys. Rev. B* **50** 11629
[67] Liu C R, Huang L, Luo H and Lai Y C 2020 *Phys. Rev. Appl.* **13** 034061
[68] Van Wees B J V, Van Houten H, Beenakker C W J, Williamson J G, Kouwen-hoven L P, van der Marel D and Foxon C T 1988 *Phys. Rev. Lett.* **60** 848
[69] Debray P, Raichev O E, Vasilopoulos P, Rahman M, Perrin R and Mitchell W C 2000 *Phys. Rev. B* **61** 10950
[70] Ouisse T 2008 *Electron Transport in Nanostructures and Mesoscopic Devices* (New York: Wiley-ISTE)
[71] Zhu R 2012 *J. Phys.: Condens. Matter* **25** 036001